Tool wear evaluation of self-propelled rotary tool and conventional round tool during turning Inconel 718

Nitin Motgi
Vishwakarma Institute of Information Technology; Dr. D.Y. Patil Institute of Engineering, Management and Research, Pune-411044, India
nitin.221p0031@viit.ac.in, http://orcid.org/0000-0001-9062-8341

Satish Chinchanikar
Mechanical department, Vishwakarma Institute of Technology, Pune, India
satish.chinchanikar@vit.edu, http://orcid.org/0000-0002-4175-3098

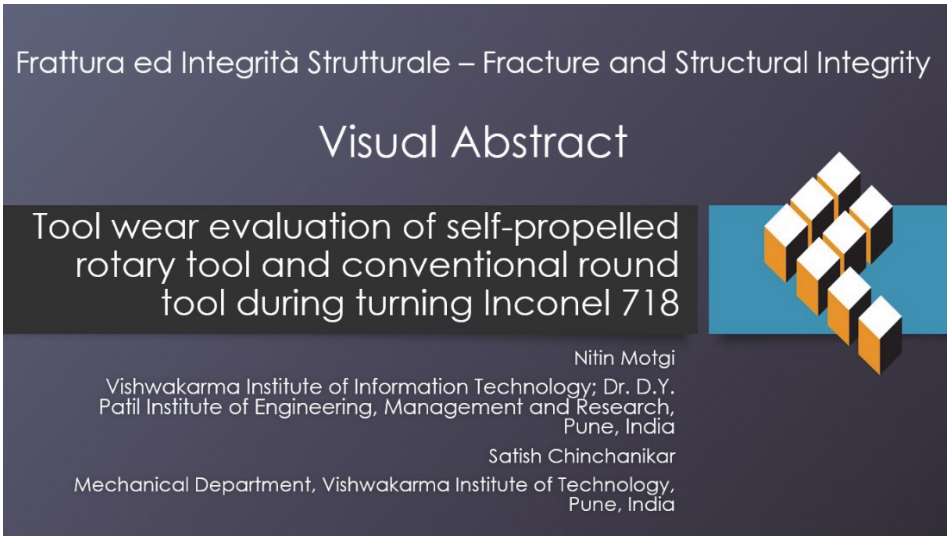

Citation: Motgi, N., Chinchanikar, S.,Tool wear evaluation of self-propelled rotary tool and conventional round tool during turning Inconel 718, Frattura ed Integrità Strutturale, 70 (2024) 242-256.

Received: 23.07.2024
Accepted: 04.08.2024
Published: 05.09.2024
Issue: 10.2024

KEYWORDS. Self-propelled rotary tools, Inconel 718, Adhesion, Tool wear, Modeling, Neural networks.

INTRODUCTION

Inconel 718, renowned for its strength, resistance to chemicals, and wear, is frequently used in aerospace manufacturing, but excessive tool wear poses challenges in machining. Predicting tool wear progression is essential in the era of sustainable machining, as it impacts dimensional accuracy, surface finish, and machining economy by affecting tool

replacement well before tool life. Researchers are working on understanding tool wear, particularly flank wear, to improve dimensional accuracy and product quality. To address this issue, manufacturers are constantly looking for cutting-edge techniques and technologies that will increase productivity and save expenses [1–2]. When machining these materials, proper cooling and lubrication techniques are essential to avoid problems like poor surface quality, workpiece dimensional and geometric accuracy, tool wear, and tool life [3-5].

Various single-layer, multi-layer, nano-composite, etc. coatings are made accessible for improved performance of cutting tools due to advancements in coating materials and technology. Most studies utilized TiAlN and AlTiN coated tools for machining Inconel 718 due to their superior oxidation resistance properties [6-7]. Flood cooling can address machinability issues, but legislative restrictions limit its use. Nanofluids are being used to enhance efficiency, with base fluid type and nanoparticle concentration influencing the process [8].

A group of researchers found PVD-coated TiAlN-TiN carbide tools improved tool life and surface roughness in machining Inconel 625 using nanofluid, possibly due to tribofilm formation [9-10]. Liquid nitrogen cooling is found to be more effective in machining nickel alloys compared to nanofluids, reducing tool wear and groove formation under minimal lubrication [11]. However, on machine components, the cryogenic environment does have certain drawbacks. Attempts were also made in machining with MoS2 and graphite-assisted MQL and with micro-textured cutting tools [12-14].

Numerous investigations have been carried out on machining using a rotary tool. When it comes to machining hardened materials, non-traditional rotary tools have demonstrated promise, leading to longer tool life and a better surface finish. The self-propelled rotary tool (SPRT) is a tool that rotates its cutting insert around its axis, demonstrating its effective use. This extra motion enhances tool performance and longevity by ensuring a more uniform distribution of heat and wear on the cutting edge [15].

When machining aerospace materials, cemented carbide SPRTs outperformed conventional round tools (CRTs) in terms of wear resistance. Research shows a sixty-fold tool life increase due to improved heat transmission during rotary cutting, reduced effective cutting speed, and steady wear distribution [16]. Kishawy et al. [17] observed that SPRT created greater surface quality, better tool life, and lower cutting forces compared to a CRT. Research shows that selecting the right inclination angle is crucial for aligning the primary cutting force with the highest stiffness of the SPRT [18].

A group of researchers observed better performance and an equal distribution of tool wear on the cutting tool's peripherals with a built and prototyped SPRT in comparison to a CRT [19]. Uhlmanna et al.'s [20] studies found that higher cutting speeds and chip cross-sectional areas caused the SPRTs to vibrate more noisily, especially while machining Inconel 718. The issue was attributed to the insufficient stiffness of the integrated bearing unit, leading to chatter, and cutting tool chipping. Research indicates that machining with SPRT significantly hardens the machined subsurface area and prolongs tool life by seven times compared to fixed tool machining. Ezugwu's [21] research shows Inconel 718's performance gain with SPRTs is lower due to its fast work hardening, negatively impacting tool life. Moreover, SPRT needs to be sufficiently stiff to avoid machining surface waviness and insert run-out. Thus, it is imperative to discover a remedy for tool chattering when machining at higher speeds [22].

A group of researchers attempted to model and optimize the complex, nonlinear wear behavior of cutting tools during machining using a promising artificial neural network (ANN) technique [23-25]. Therefore, it will be advantageous to develop a reliable flank wear growth model. Research indicates that both the volume and caliber of data used for training affect its efficacy. The development of ANN models for predicting machining performance has been accomplished; however, modeling the flank wear evolution of SPRTs during Inconel 718 turning has not been attempted.

Based on the literature review, it can be inferred that utilizing SPRTs during machining has several advantages over using CRTs. These advantages include longer tool life, reduced cutting temperatures, an increased metal removal rate, and enhanced machinability. However, the widespread use of these tools in the metalworking industry is still limited. Moreover, few studies have attempted to determine the flank wear progression of SPRTs during machining Inconel 718.

With this view, this work evaluates the tool wear and its progression through mathematical modeling during turning Inconel 718 using SPRTs and CRTs. Experiments were performed by varying the cutting parameters. Tool wear was measured and analyzed using scanning electron and digital microscopes. Mathematical models were developed to analyze and comparatively evaluate the effect of cutting parameters and machining time on the tool wear of SPRTs and CRTs. Furthermore, since the ANN is a promising method for mathematically simulating complex, nonlinear wear behavior, a model to predict the progression of flank wear was developed for the best performing tool. Finally, tool wear mechanisms for SPRTs and CRTs are discussed, and a summary of the work is presented.

EXPERIMENTAL DESIGN

Flank wear, wear mechanisms, and tool life were examined during turning Inconel 718 with a self-propelled rotary tool (SPRT) and a conventional round tool (CRT) on a CNC lathe. Following an extensive review of the literature, pilot testing, machine capacity, and tool manufacturer recommendations, the process parameters for the chosen tool-workpiece combination were carefully selected. In these experiments, 70 mm diameter, 400 mm length, and 37 HRC hardness Inconel 718 were employed. Fig. 1 shows the percentage of each element's chemical makeup in Inconel 718.

C	0.005	Mn	0.062	S	0.007	Mo	2.87	Al	0.35	Nb+Ta	5.01	B	0.001
Si	0.056	P	0.008	Cr	18.37	Ni	52.82	Co	0.22	Ti	1.10	Fe	Balance

Figure 1: Percentage of each element's chemical makeup in Inconel 718.

The experimental matrix used to compare the tool wear for a CRT and an SPRT is displayed in Tab. 1. Cutting speed had to be restricted to 65 m/min because, even with the lowest feed and depth of cut values, premature tool failure happened, particularly for CRTs, above this speed. The present study makes use of a cemented carbide round tool or round insert, designated as RCMT1606M0MP, with dimensions of 16 mm in diameter, 6 mm in thickness, and a 7° relief angle. The M0MP chip breaker design effectively manages chip formation and evacuation during cutting, ensuring efficient machining and maintaining surface finish quality.

Experimental run	R1	R2	R3	R4	R5	R6	R7	R8	R9
Cutting speed (V) (m/min)	30	30	65	65	50	30	30	65	65
Feed (f) (mm/rev)	0.1	0.3	0.1	0.3	0.2	0.1	0.3	0.1	0.3
Depth of cut (d) (mm)	0.8	0.8	0.8	0.8	0.5	0.2	0.2	0.2	0.2

Table 1: Experimental matrix.

A customized right-handed tool holder was used to hold a CRT. The customized tool holder prioritizes stability and adaptability in cutting while offering a strong grip for inserts. This tool holder has a 7° clearance angle, and the circular insert was held in place with a lever lock mechanism. Similarly, a customized right-handed tool holder was used for turning with a SPRT. Fig. 2 depicts a SPRT with assembly details. The tool holder of SPRT has an inclination angle of 6° and a rake angle of 35°. A system of needle bearings and thrust bearings was preloaded to support the rotating circular insert shaft.

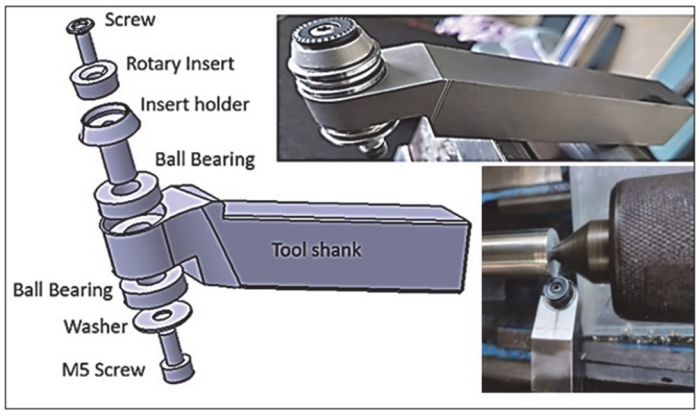

Figure 2: Self-propelled rotary tool (SPRT) with assembly details.

RESULTS AND DISCUSSION

This section discusses the evaluation of flank wear of SPRT and CRT during turning Inconel 718 by developing mathematical models. Tools with varying wear patterns are described using scanning electron microscopy (SEM) and digital microscopy images. The research work gives the industrial community vital information that they can use to decide on tool replacement guidelines and limitations on metal machining cutting conditions.

The flank wear was monitored up to a flank wear length of 0.2 mm, as beyond this value, cutting edge chipping rather than steady expansion of flank wear was the cause of tool failure. when machining Inconel 718 [24]. Figs. 3 and 4 show the flank wear growth for the SPRTs and CRTs, respectively, for cutting conditions, as shown in Tab. 1. Plots indicate that early breakdown, consistent wear rate, and rapid cutting-edge breakdown are the three main regions of flank wear. With cutting time, the flank wear increases. Different patterns of flank wear growth are seen in the tools from experimental runs 1 to 9. While some tools show a more uniform wear rate, others show rapid wear at the cutting edge. Both SPRT and CRT in run R4 experienced the most rapid flank wear growth, reaching the quick cutting-edge breakdown stage in a relatively short amount of time for both tools. With CRTs, this effect may be viewed as being more noteworthy. In contrast, both tools in run 6 exhibited a more gradual increase in flank wear, indicating a more uniform wear rate over time. Additionally, SPRTs make this effect very noticeable.

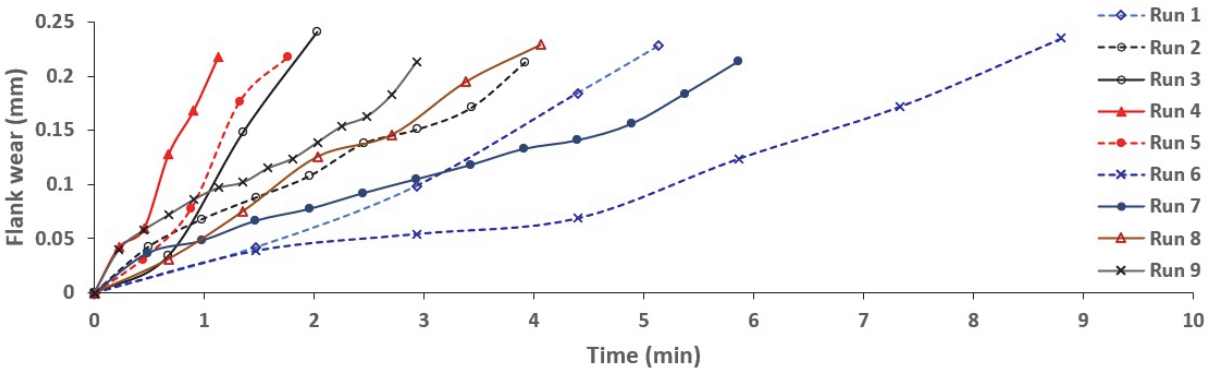

Figure 3: Flank wear progression of SPRTs for experimental runs as depicted in Tab. 1.

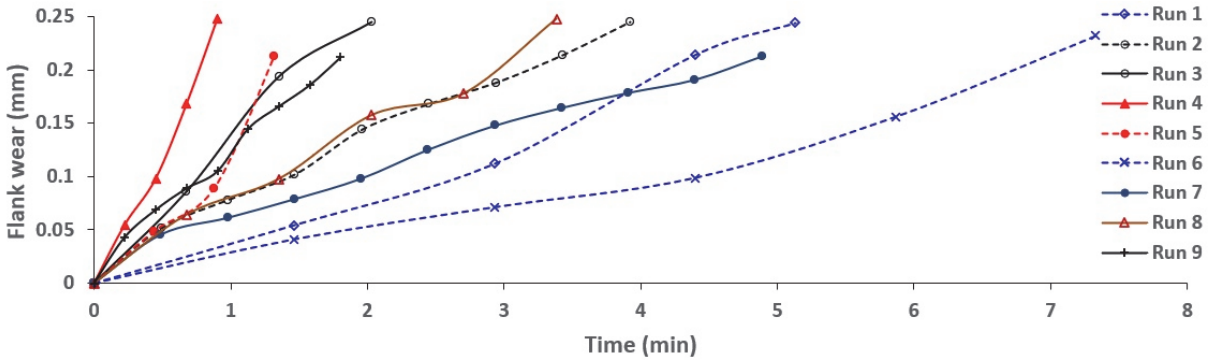

Figure 4: Flank wear progression of CRTs for experimental runs as depicted in Tab. 1.

Small fractures and micro-chipping result from the cutting tool's initial breakdown when it meets the workpiece material. The tool reaches a stable condition when progressive abrasion and friction produce a consistent wear pattern, which is known as the uniform wear rate area. As a result of greater temperatures and stronger pressures during extended cutting operations, fast cutting-edge failure is also characterized by accelerated wear. Experiments revealed that the primary cause of tool failure, especially for CRTs, is cutting edge chipping above 0.2 mm flank wear. Fig. 5 displays tool images showing tool wear at the end of tool life at experimental run 4 for SPRTs and CRTs.

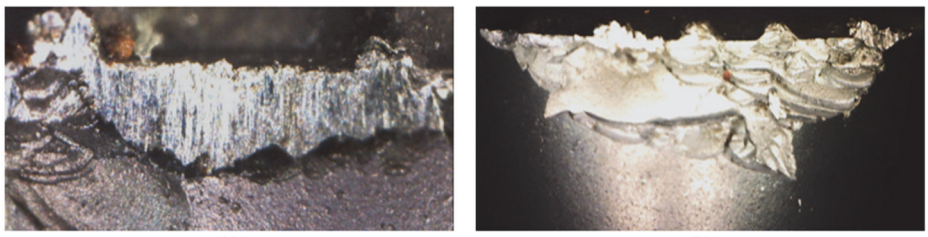

Figure 5: Flank wear images at the end of tool life at experimental run 4 for (a) SPRT, (b) CRT.

Similarly, Figs. 6-7 display tool images showing tool wear at the end of tool life at experimental runs 1, 2, 8, and 9 for SPRTs and CRTs. Cutting edge chipping and catastrophic failure were found to occur at higher cutting speeds, while flank wear predominated at lower cutting speeds. But for CRTs, this effect was noteworthy. The main kind of tool deterioration at lower speeds was found to be flank wear, which suggests that the cutting edge gradually wore down. Chipping of the cutting edge becomes increasingly noticeable as speed rises, indicating that the cutting edge cannot handle the increased pressures and stresses. Eventually, catastrophic failure became apparent at greater speeds, signifying a total tool breakdown.

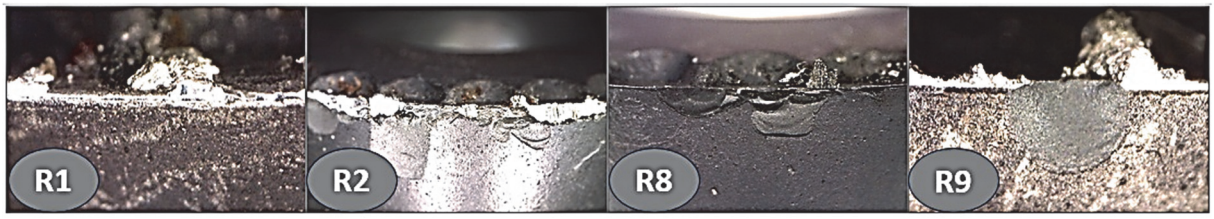

Figure 6: Flank wear images at the end of tool life for SPRTs at experimental runs 1, 2, 8, and 9.

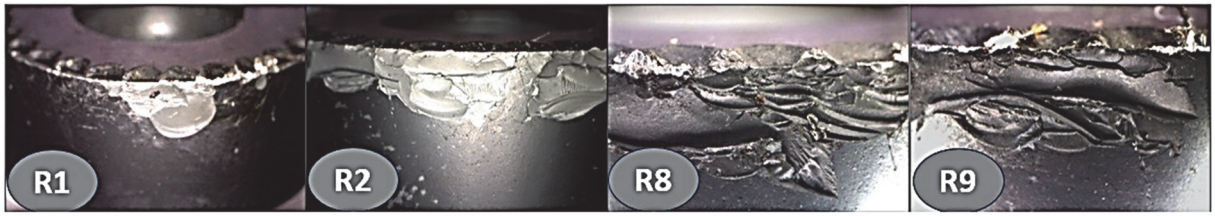

Figure 7: Flank wear images at the end of tool life for CRTs at experimental runs 1, 2, 8, and 9.

To estimate the flank wear of SPRT and CRT, mathematical models were created, considering the influence of the cutting conditions and the machining time. Tool wear observations collected at various machining periods and under various cutting circumstances were used to develop a model (Figs. 3 and 4). The unknown constants in Eq. (1) were obtained by minimizing the least square error between the experimental and anticipated flank wear values. Excel's Analysis ToolPak, which provides advanced data analysis tools, was used to obtain the flank wear regression equations and perform multiple regression analyses for SPRTs and CRTs. These tools offer a straightforward way to perform advanced data analysis without needing specialized software. It quickly generates statistical analysis results directly in Excel and provides a wide range of analysis tools suitable for various types of data analysis. In total 111 flank wear values (around 61 for SPRTs and 50 observations for CRTs) measured at different cutting conditions and machining times (t) (Figs. 3 and 4) were used to develop flank wear regression equations. The regression output included the regression equation, R-squared value, and significance levels (p-values) for the flank wear mathematical models. The final flank wear growth equations for SPRT and CRT are shown by Eqs. (2) and (3), respectively.

$$VB = k_0 V^{p} f^{q} d^{r} t^{s} \tag{1}$$

$$VB_{SPRT} = 0.004436 V^{0.976} f^{0.401} d^{0.338} t^{0.833} \tag{2}$$

$$VB_{CRT} = 0.003012 V^{1.1599} f^{0.4517} d^{0.295} t^{0.8381} \tag{3}$$

The flank wear (VB) is influenced by cutting speed (V), feed (f), depth of cut (d), and machining time (t) according to the given equations. k_0, p, q, r, and s are constants. The constants p, q, r, and s determine the impact of V, f, d, and t on the flank wear, respectively.

Regression statistics and ANOVA for flank wear models of SPRT and CRT are shown in Tab. 2. In regression analysis, several key statistics are used to evaluate the fit and explanatory power of the model. The multiple R shows the correlation coefficient between the observed and predicted flank wear, and a value closer to plus or minus one indicates a strong linear relationship. R square measures the proportion of the variance in the predicted results, and a value close to 1 indicates that the model explains better variability. Adjusted R square provides a more accurate measure of the model's explanatory power. The standard error measures the standard deviation of the residuals (prediction errors).

	Regression statistics				
	Multiple R	R Square	Adjusted R Square	Standard Error	No. of observations
SPRT	0.928	0.862	0.852	0.228	61
CRT	0.966	0.933	0.927	0.147	50
	ANOVA				
		Degrees of freedom (df)	Sum of squares (SS)	Mean square (MS)	F-value	Significance F (p-value)
SPRT	Regression	4	18.341	4.585	87.784	1.89×10^{-23}
	Residual	56	2.925	0.052		
	Total	60	21.266			
CRT	Regression	4	13.692	3.423	157.792	7.3×10^{-26}
	Residual	45	0.976	0.021		
	Total	49	14.668			

Table 2: Regression statistics and ANOVA for flank wear model of SPRT and CRT.

A low p-value (typically less than 0.05) indicates that the developed models are significant. Multiple R and R square values of 0.928 and 0.862, respectively, for SPRT and 0.933 and 0.927, respectively, for CRT indicate that the developed mathematical models could be used to assess the flank wear of SPRTs and CRTs during the turning of Inconel 718 within the range of the chosen process parameters.

In Fig. 8, flank wear development throughout a 3-minute machining period is shown, considering the influence of cutting parameters. A single input parameter was changed, while the other two parameters were held constant to predict the flank wear results. The first section of the plot shows estimated flank wear varying with V at f and d values of 0.2 mm/rev and 0.5 mm, respectively. The middle section shows the flank wear values varying with f at a V and d of 50 m/min and 0.5 mm, respectively. The last section of the plot shows the estimated flank wear varying with d at a V and f of 50 m/min and 0.2 mm/rev, respectively.

Flank wear is significantly affected by the V, followed by the t, f, and d. This can also be confirmed by the higher exponent values for the V, followed by the t, f, and d in Eqs. (2) and (3). Furthermore, with CRTs compared to SPRTs, a notable influence of the cutting conditions on flank wear is seen. The greater exponent values for the cutting parameters in Eq. (3) as opposed to Eq. (2) further support this. Further, flank wear progression was simulated for SPRTs and CRTs under cutting circumstances as shown in Tab. 3.

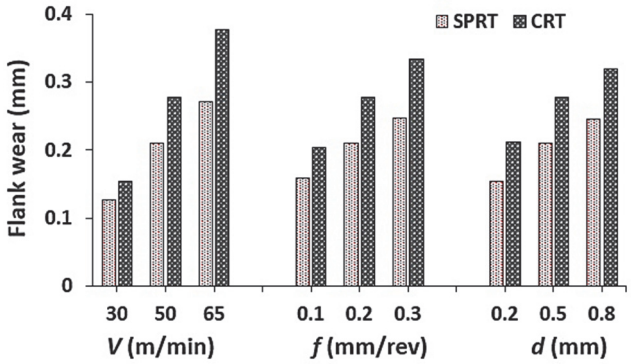

Figure 8: Comparative flank wear progression for SPRT and CRT varying with cutting parameters.

Cutting parameters	Experimental run											
	SPRT						CRT					
	SS1	SS2	SS3	SS4	SS5	SS6	SC1	SC2	SC3	SC4	SC5	SC6
V (m/min)	30	65	50	50	50	50	30	65	50	50	50	50
f (mm/rev)	0.2	0.2	0.1	0.3	0.2	0.2	0.2	0.2	0.1	0.3	0.2	0.2
d (mm)	0.5	0.5	0.5	0.5	0.2	0.8	0.5	0.5	0.5	0.5	0.2	0.8

Table 3: Cutting conditions used for simulating flank wear progression for SPRT and CRT.

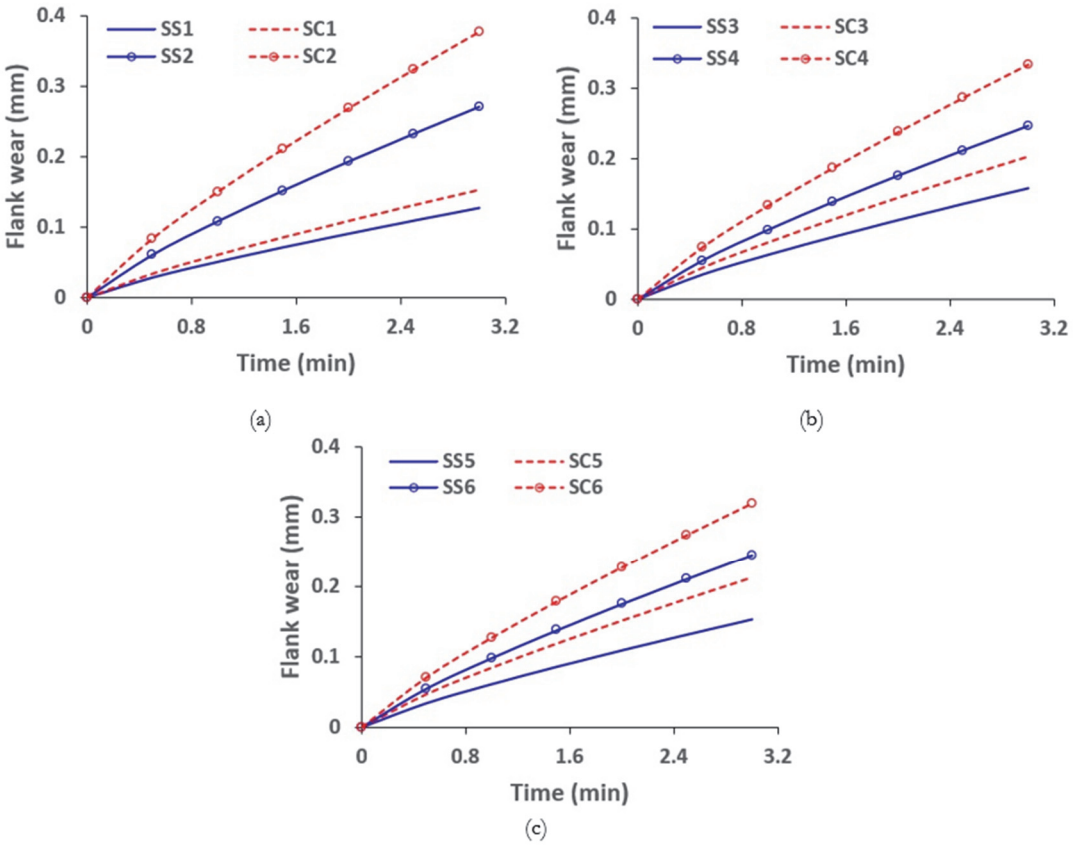

Figure 9: Simulated flank wear progression for SPRT and CRT at cutting conditions (a) SS1/SC1, SS2/SC2, (b) SS3/SC3, SS4/SC4, and (c) SS5/SC5, SS6/SC6.

The established flank wear equations were reduced to two parameter levels, allowing flank wear to be estimated over a variety of input values. Plots are made between the machining time and the estimated evolution of flank wear. Fig. 9(a) shows the flank wear progression for two different cutting speeds, namely 30 and 65 m/min, and at feed and depth of cut of 0.2 mm/rev and 0.5 mm, respectively. The flank wear growth for CRTs can be seen to be steeper at higher cutting speeds as compared to SPRT. However, a comparatively lower distinctive effect on the flank wear growth of SPRTs and CRTs can be seen when varying with feed (Fig. 9(b)) and an almost negligible effect when varying with depth of cut (Fig. 9(c)). This can also be confirmed from Eqs. (2) and (3), which show a distinctive difference in exponent values for cutting speed, followed by a comparatively smaller difference in exponent values for feed and almost similar values for depth of cut.

It is well noted that as cutting parameters increase, so does tool wear. As shown in Fig. 9(a), the flank wear does, in fact, increase noticeably with the cutting speed and cutting duration. However, this effect can be seen more prominently for CRTs. The fact that the cutting speed exponent in Eqs. (2) and (3) is higher for CRTs than it is for the other parameters lends support to this. The rise in flank wear at faster cutting speeds and longer cutting durations might be attributed to the development of higher cutting temperatures, which enhance the rate of flank wear. However, the self-propelled rotary motion of the cutting insert allowed for cooling of the cutting edge and prevented faster growth of the tool wear due to high temperature activated wear mechanisms.

This study found that cutting speed had the largest impact on tool flank wear, with machining time, feed, and depth of cut following closely behind. However, this effect was more prominent for CRTs than SPRTs. Higher tool lives of 7.56 and 6.78 minutes can be seen as obtained for SPRT and CRT, respectively, at experimental run 6. Lower tool lives of 0.91 and 0.78 minutes can be seen for SPRT and CRT, respectively, at experimental run 4. In this condition, the tool failed because the fast-moving chips broke the attached metal, causing cutting edge chipping. It is obvious that longer tool life results from lower cutting speeds. Monitoring the development of tool wear can help prevent catastrophic tool failures and the resulting damage to the machined workpiece and machine tools.

Figs. 10(a) and (b) display the observed and anticipated flank wear for SPRT and CRT at experimental run 6. Clearly, there is a fair degree of agreement between the observed and predicted flank wear. However, deviations were seen for both the tools above the flank wear of 0.2 mm due to cutting edge chipping instead of the gradual tool wear almost for all the cutting

conditions used in the present study. This could be due to after prolonged machining, the adhered material with the tool flank dislodges, leading to cutting edge chipping or pitting on the tool faces.

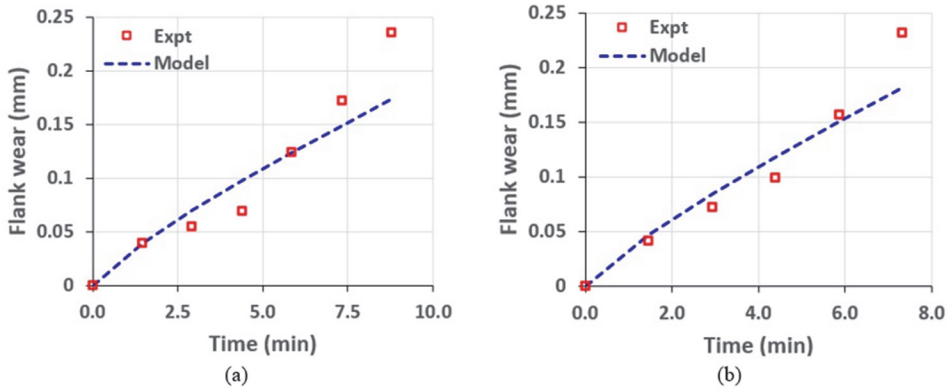

Figure 10: Experimental vs anticipated flank wear at experimental run 6 for (a) SPRT, (b) CRT.

This study found a 67% increase in tool life for SPRTs over CRTs, especially at a higher cutting speed of 65 m/min, due to improved heat transmission and steady wear distribution. But at lower cutting conditions, the tool life gain was only 15–18%, indicating that SPRTs could be reliably used at higher cutting conditions to achieve machining economy. Additionally, SPRTs exhibited better chip control and reduced built-up edge formation than CRTs.

From the experimental investigations, this study found that SPRTs may be a more cost-effective option for machining operations with higher cutting speeds while machining Inconel 718. Nonetheless, the 0.2 mm tool wear criteria are more practical since, at this threshold, cutting edge chipping rather than gradual flank wear progression led to tool failure. Therefore, to assure dimensional accuracy and surface smoothness, the proposed flank wear models may be utilized with confidence to anticipate the development of flank wear up to a flank wear length of 0.2 mm. Overall, the results suggest that SPRTs are a more efficient and cost-effective option for machining operations, particularly at higher cutting speeds. The improved heat transmission and wear distribution of SPRTs contribute to their superior performance in comparison to CRTs.

Further, digital and SEM images were used to analyze the mechanisms and forms of tool wear of a particular tool when turning Inconel 718. The three primary wear patterns found were distortion of the cutting edge, chipping of the edge, and flank wear. Fig. 11 depicts the tool wear images at the end of the tool life at experimental run 3. Compared to the SPRTs (Fig. 11(a)), the CRTs (Fig. 11(b)) exhibit much more pitting, metal adhesion, and chipping of the cutting edge. This indicates that the CRTs experienced more severe wear and deformation during cutting operations compared to the SPRTs. The adherence of metal can impede smooth functioning and create friction; while chipping and pitting weaken the cutting edge. Additionally, uneven surfaces caused by chipping and pitting reduce efficiency and precision. Fig. 12 depicts the tool wear images at the end of the tool life at experimental run 5. Under a magnifying lens, tiny abrasive scratches and metal adhering to the tool are visible. This stubborn metal was removed after extensive cutting, damaging the tool faces in the process. Tool integrity is compromised by pitting on tool faces caused by metal adhesion and dislodgement, which also shortens the tool's lifespan and effectiveness.

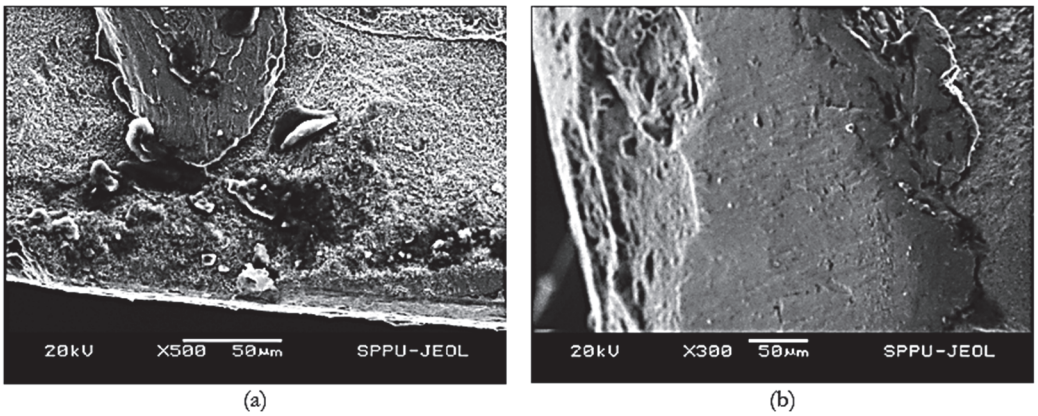

Figure 11: SEM images of tools for experimental run 3 (a) SPRT, (b) CRT.

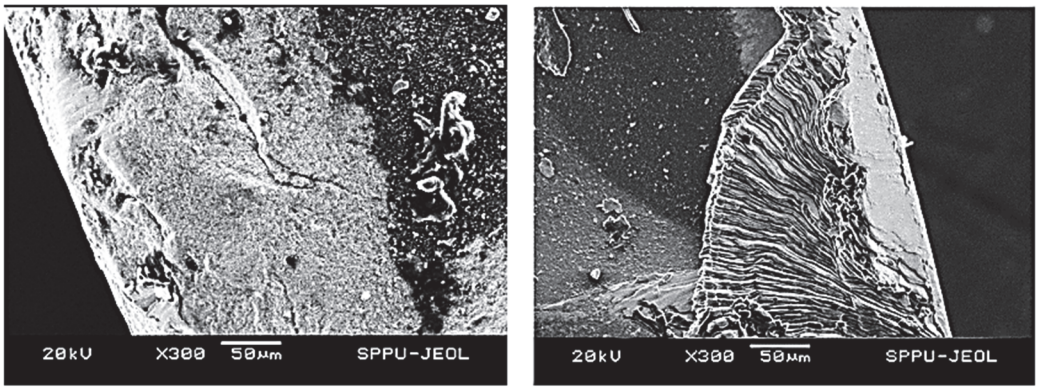

Figure 12: SEM images of tools for experimental run 5 (a) SPRT, (b) CRT.

Tool fractures resulting from the plucking of the attached material were prominently seen in CRTs, and comparatively lower adhesion and damage to the tool were seen in SPRTs. The higher friction and stress produced during machining with CRTs is the cause of this plucking phenomenon. Harder tool particles exacerbate tool wear and eventually cause fractures. Adhesive wear is the term for this kind of wear, in which the hard tool flank particles stick to the machined surface and generate friction. This suggests that adhesion becomes a major influence on tool wear at higher cutting speeds. Adhesion indicates that more tool wear is likely to occur since the workpiece and tool materials are bonding together during the cutting operation. The cutting edge was distorted plastically due to the increased cutting speeds and strong compressive forces. The two main wear processes observed on the substrate were adhesion and pitting. The cutting edge was spoiled due to increased loads and cutting temperatures, resulting in plastic deformation during the resumption of the machining.

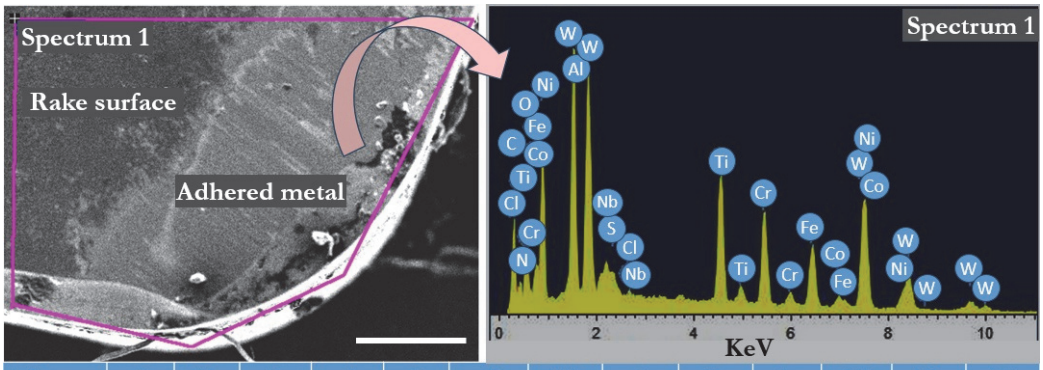

Element	C	N	O	Al	S	Cl	Ti	Cr	Fe	Co	Ni	Nb	W
Weight%	28.83	13.47	10.10	5.05	0.26	0.15	5.20	5.10	4.58	0.95	12.18	1.20	12.93

Figure 13: SEM image of rake surface of CRT tool with EDS for experimental run 8.

When utilizing a CRT at a higher cutting speed (experimental run 8), Fig. 13 shows the attachment of workpiece material to the tool rake surface, a plastically warped and ruined cutting edge, and pitting. This suggests that cutting speed plays a crucial role in determining the extent of tool wear and workpiece material adhesion during machining processes. For SPRT, this impact was also noted. Its impact was, nonetheless, less noteworthy than that of CRT. The findings suggest that CRT at higher cutting speeds results in more severe tool wear and workpiece material attachment compared to SPRT.
This study identifies areas for future investigation in SPRTs, considering the effect of process parameters under different cooling conditions on the extensive use of these tools in metalworking. The following section discusses the development of an ANN model to predict tool wear for the best performing SPRT tool during turning Inconel 718.

ANN model

The ANN model, derived from the biological nervous system, is a computational tool used to simulate complex, nonlinear wear behavior in real-world interactions. ANN simulates input parameters and output responses, with a fully linked multi-layer perceptron (MLP) being an example. MLP consists of three layers: input, hidden, and output, each with interconnected artificial neurons. The input layer receives raw input, while the hidden layer processes input data and sends the outcome to

the output layer. More details on the architecture of a neural network requiring preprocessing of input features, initialization of weights, bias addition, and selection of activation functions can be referred to in [25]. A typical ANN architecture and a flow chart showing the step-by-step procedure for the ANN tool wear modeling are depicted in Fig. 14.

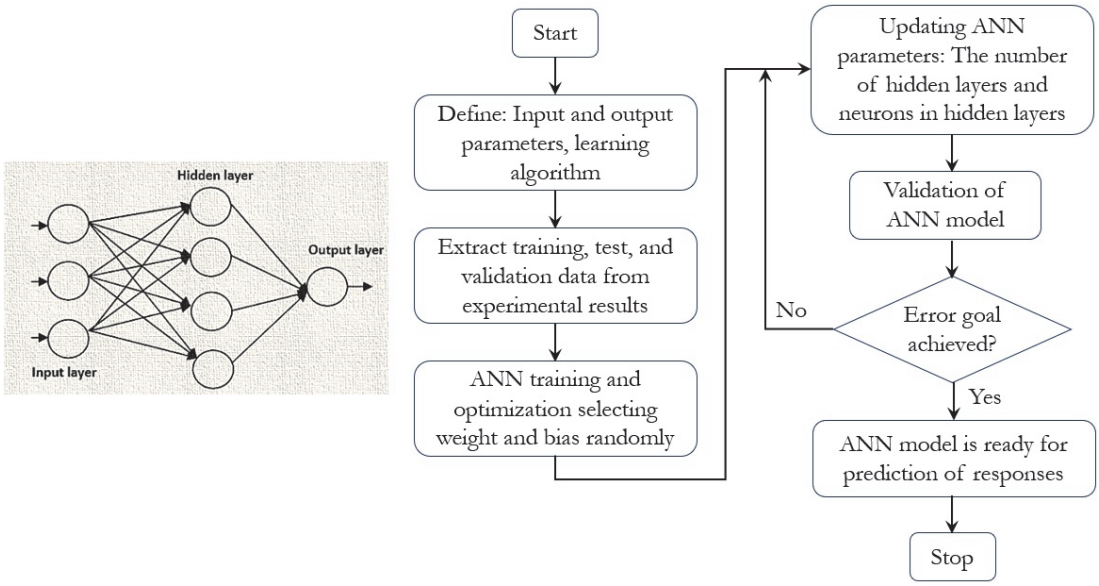

Figure 14: Typical ANN architecture and the step-by-step procedure for the ANN tool wear modeling [25].

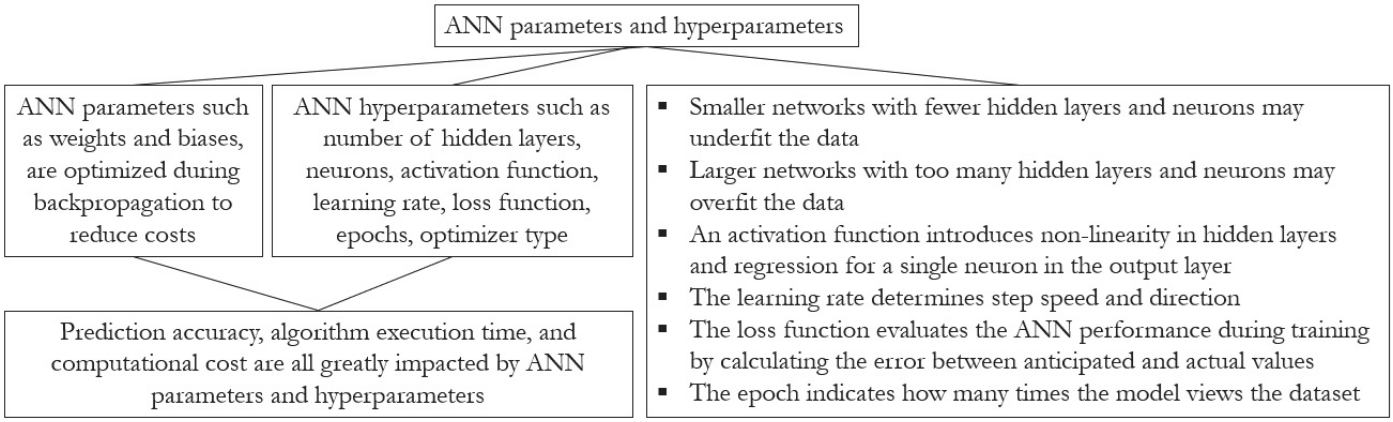

Figure 15: ANN parameters and hyperparameters

The ANN parameters and hyperparameters, as seen in Fig. 15, must be optimized as they have a substantial influence on computing cost and prediction accuracy. The MATLAB Toolbox was used in this work to create the flank wear ANN model. Four neurons are in the input layer to measure V, f, d, and t; one neuron is in the output layer to forecast flank wear. A feed-forward neural network maps numerical inputs to numerical targets, selecting a two-layer network with sufficient neurons in the hidden layer and a linear output neuron at random. The ANN architecture to get flank wear is shown in Fig. 16.

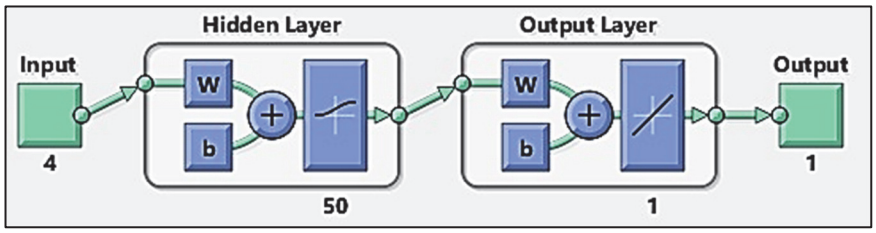

Figure 16: The ANN architecture for flank wear.

By altering the quantity of neurons and hidden layers, the study built several ANN networks. Plotting tests and training errors versus epochs were used to evaluate the effectiveness of ANN networks. The current study's default parameters for the learning rate and maximum number of epochs were 1000 and 0.01, respectively. There was no restriction on computation time for creating an ANN model. It has an endless time setting. Fig. 17 provides the ANN parameters used in the design and analysis.

Figure 17: ANN model parameters.

For network training, scaled conjugate gradient methods, Bayesian regularization, and the Levenberg-Marquardt approach can be applied. Due to its faster speed compared to other algorithms, the Levenberg-Marquardt approach has been employed in this work. A key element in neural networks that adds non-linearity to the model and enables it to learn from intricate data patterns is the transfer function, also known as the activation function. TANSIG (tangent-sigmoid) and LOGSIG (log-sigmoid) are two often utilized transfer functions. LOGSIG and TANSIG transfer functions are commonly employed in hidden layers as they introduce non-linearity. In practice, the choice between LOGSIG and TANSIG depends on the specific problem and the architecture of the neural network. The PURELIN transfer function is used to obtain a linear relationship between the input and output, and the network needs to output a continuous value.
In this study, the ANN flank wear model performance was assessed using the hyperbolic tangent-sigmoid (tansig) and log-sigmoid (logsig) transfer functions at the hidden layer, respectively, and the PURELIN transfer function at the output layer as shown in Fig. 16. In contrast to the hyperbolic tangent-sigmoid (tansig) transfer function, this study revealed that the log-sigmoid (logsig) transfer function, as given by Eq. (4), improved ANN performance.

$$f(N) = \text{logsig}(x) = \frac{1}{1+e^{-x}} \tag{4}$$

The ANN model for SPRT is created by examining flank wear values from Fig. 3. The ANN SPRT model's performance was assessed by changing the quantity of hidden layers and neurons within them. One common method for determining when neural network models will converge is to analyze learning curve graphs. Usually, a graph showing losses against epochs is shown. It is expected that accuracy will grow and loss will decrease with an increase in training epochs. But eventually, they will settle down. A neural network ultimately strives for convergence over multiple training epochs. Regression coefficient (R) values, computational time, and mean squared error were employed as performance metrics to determine which model performed best.
The ANN model with one hidden layer and fifty neurons produced better performance, as shown in Fig. 18. Epoch 5 saw the highest validation performance, with a score of 14.623×10^{-5} and a prediction accuracy of 0.97945. Fig. 19 displays the ANN model regression coefficients discovered for the full data set as well as during model testing, validation, and training. The developed artificial neural network model has regression coefficient values close to one.

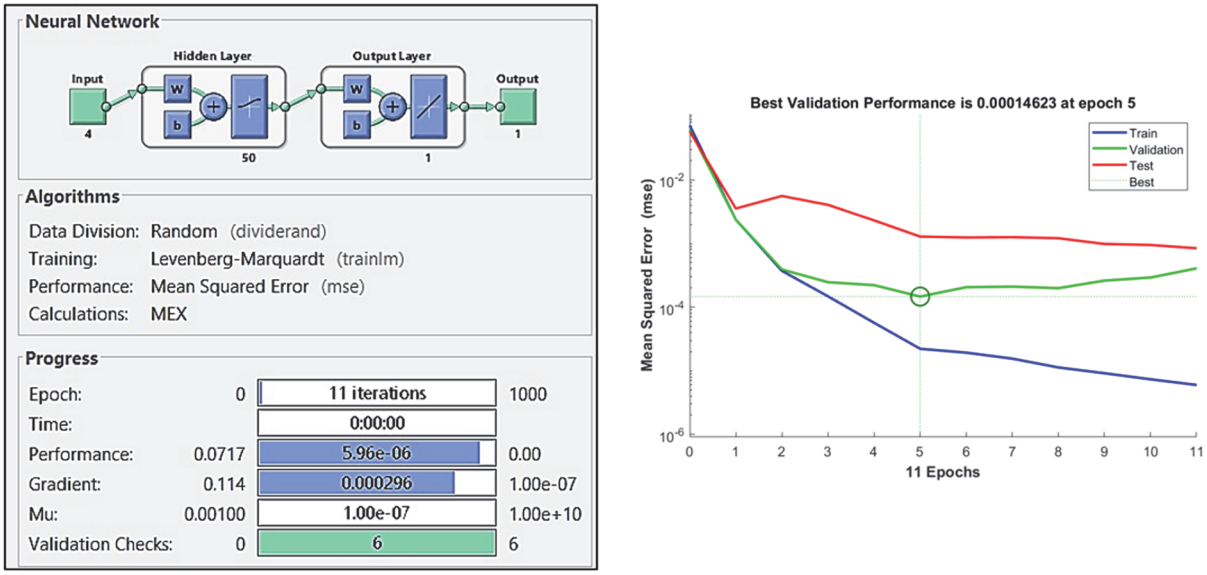

Figure 18: The ANN SPRT model's performance.

Regression coefficients close to one indicate that the developed ANN model could be used to predict the flank wear of SPRT when turning Inconel 718. Further, the accuracy of the ANN model was assessed through validatory experiments at different cutting conditions and machining times, excluding those used for model development. Using ANN and mathematical models, Fig. 20 compares experimental and expected flank wear under the cutting circumstances shown in Tab. 4. It is evident that predicted outcomes from ANN models agree more closely with experimental values compared to mathematical models.

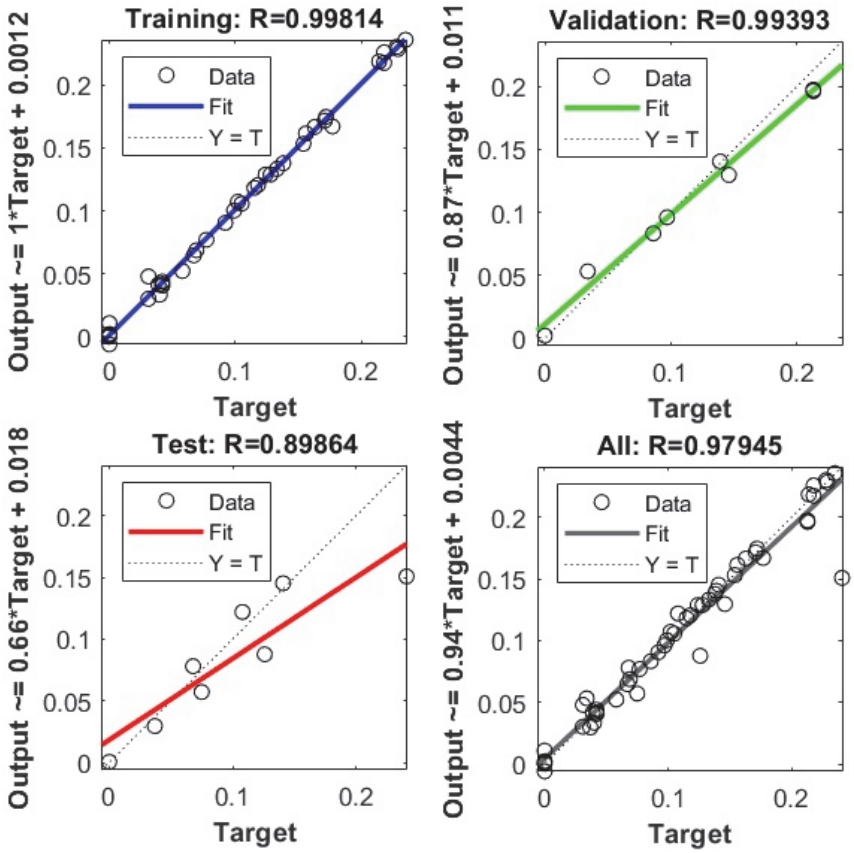

Figure 19: ANN regression coefficients.

Cutting parameters	Validatory expt. run													
	1	2	3	4	5	6	7	8	9	10	11	12	13	14
V (m/min)	30	30	30	65	65	65	50	30	30	30	30	65	65	65
f (mm/rev)	0.1	0.3	0.3	0.1	0.3	0.3	0.2	0.1	0.1	0.3	0.3	0.1	0.3	0.3
d (mm)	0.8	0.8	0.8	0.8	0.8	0.8	0.5	0.2	0.2	0.2	0.2	0.2	0.2	0.2
t (min)	4.4	1.47	2.94	1.35	0.45	0.9	0.88	2.93	5.86	0.98	5.38	3.38	0.68	2.71

Table 4: Cutting conditions used for validating SPRTs flank wear progression.

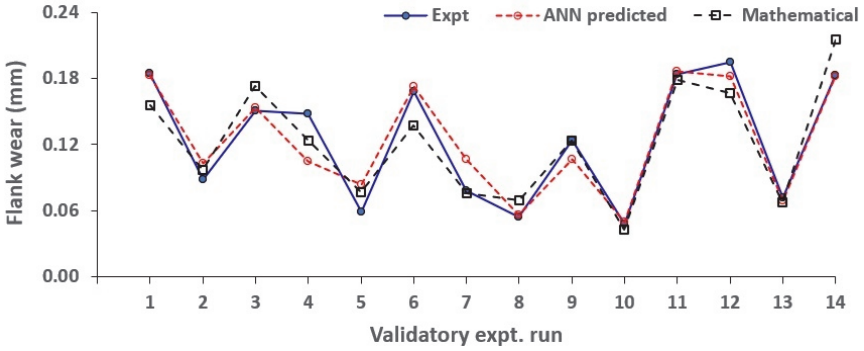

Figure 20: Experimental vs. predicted flank wear.

According to this investigation, there is high agreement between the anticipated and observed flank wear values up to 0.2 mm of flank wear. But in most cutting scenarios with flank wear beyond 0.2 mm, extended cutting leads to metal adhesion and dislodgement, which chips the cutting edge and damages the tool faces. Therefore, to achieve improved surface quality and dimensional precision while machining Inconel 718 using SPRTs, it is more practical to use the tool wear criteria of 0.2 mm. This study finds a scope for further research in SPRTs on the widespread use of these tools in the metalworking industry. Further investigation into the impact of varying cooling conditions on the performance and longevity of SPRTs could provide valuable insights for optimizing their efficiency in industrial applications. Additionally, exploring how different materials respond to these process parameters could offer a comprehensive understanding of their overall effectiveness in metalworking operations.

CONCLUSIONS

In this work, the tool wear of self-propelled rotary tools (SPRTs) and conventional round tools (CRTs) during Inconel 718 turning is compared. The tool wear progression was simulated under different cutting circumstances for both tools by developing mathematical models. The experimental results obtained during the turning of Inconel 718 were used to calibrate and evaluate the developed flank wear progression models for SPRTs and CRTs. Further, an ANN model to predict flank wear progression was developed for the best performing tool. The experiments were designed to cover a broad range of operating conditions to ensure the model's accuracy and applicability in practical machining scenarios. The following conclusions could be drawn from the present work.

- Improved heat transmission and consistent wear distribution led to a 67% increase in tool life for SPRTs compared to CRTs, especially at higher cutting speeds of 65 m/min. This suggests that SPRTs could be used reliably at higher cutting conditions to achieve machining economy.
- The cutting speed had the largest impact on tool flank wear, with machining time, feed, and depth of cut following closely behind. However, this effect was more prominent for CRTs. On the other hand, the depth of cut was having an almost similar effect on the flank wear progression of both tools.
- The R-squared values for the developed models close to 0.9 indicate their potential utility for assessing flank wear within the limits of the chosen cutting tool and work material combination.
- Primary wear mechanisms were observed to include adhesion, substrate pitting, chipping, and cutting-edge distortion caused by increased loads and cutting temperatures. Tool fractures owing to the plucking of the attached material were prominently seen in CRTs. On the other hand, SPRTs showed significantly reduced adhesion and

tool damage, even at higher cutting conditions. SPRTs also exhibited better chip control and reduced built-up edge formation than CRTs.

- Cutting edge chipping after prolonged cutting was found to be the dominant failure mode for SPRTs due to the constant shifting of the tool edge during machining, which may cause mechanical and thermal shock.
- The created ANN model, whose regression coefficient values are nearly equal to one, indicates that it could be used to predict flank wear of SPRTs during Inconel 718 turning with accuracy.
- Compared to the mathematical model, the ANN models' projected outcomes agreed with the experimental values more closely. For the ANN and mathematical models, the average prediction error was 9.67% and 13.39%, respectively.
- Overall, SPRTs are a more efficient and cost-effective option for Inconel 718 turning operations, particularly at higher cutting speeds. The improved heat transmission and wear distribution of SPRTs contributed to their superior performance in comparison to CRTs.
- This study finds a scope for further research in SPRTs, considering the effect of process parameters under different cooling conditions on the widespread use of these tools in the metalworking industry.

REFERENCES

[1] Rajurkar, A. and Chinchanikar, S. (2024). Investigations on homothetic and hybrid micro-textured tools during turning Inconel-718. Mater. Manuf. Processes, 39(4), pp. 529-545. DOI: 10.1080/10426914.2023.2236188.

[2] Rajurkar, A. and Chinchanikar, S. (2023). Investigation on the effect of laser parameters and hatch patterns on the dimensional accuracy of micro-dimple and micro-channel texture geometries. Int. J. Interact. Des. Manuf., pp. 1-18. DOI: 10.1007/s12008-023-01258-z.

[3] Chinchanikar, S. and Choudhury, S.K. (2015). Machining of hardened steel—experimental investigations, performance modeling and cooling techniques: a review. Int. J. Mach. Tools Manuf., 89, pp. 95-109. DOI: 10.1016/j.ijmachtools.2014.11.002.

[4] Kulkarni, P. and Chinchanikar, S. (2023). A Review on Machining of Nickel-Based Superalloys Using Nanofluids Under Minimum Quantity Lubrication (NFMQL). J. Inst. Eng. India Ser. C, 104(1), pp. 183-199. DOI: 10.1007/s40032-022-00905-w.

[5] Jeyapandiajan, P. and Anthony, X.M. (2019). Evaluating the machinability of Inconel 718 under different machining condition. Procedia Manuf., 30, pp. 253-260. DOI: 10.1016/j.promfg.2019.02.037.

[6] Günan, F., Kıvak, T., Yıldırım, C.V. and Sarıkaya, M. (2020). Performance evaluation of MQL with AL2O3 mixed nanofluids prepared at different concentrations in milling of Hastelloy C276 alloy. J. Mater. Res. Technol., 9(5), pp. 10386-10400. DOI: 10.1016/j.jmrt.2020.07.018.

[7] Şirin, E., Kıvak, T. and Yıldırım, C.V. (2021). Effects of mono/hybrid nanofluid strategies and surfactants on machining performance in the drilling of Hastelloy X. Tribol. Int., 157, p. 106894. DOI: 10.1016/j.triboint.2021.106894.

[8] Chinchanikar, S., Kore, S.S. and Hujare, P. (2021). A review on nanofluids in minimum quantity lubrication machining. J. Manuf. Processes, 68(A), pp. 56-70. DOI: 10.1016/j.jmapro.2021.05.028.

[9] Yıldırım, C.V. and Sarıkaya, M. (2019). The effect of addition of hBN nanoparticles to nanofluid-MQL on tool wear patterns, tool life, roughness and temperature in turning of Ni-based Inconel 625. Tribol. Int., 134, pp. 443-456. DOI: 10.1016/j.triboint.2019.02.027.

[10] Behera, B.C., Ghosh, S. and Rao, P.V. (2016). Application of nanofluids during minimum quantity lubrication: a case study in turning process. Tribol. Int., 101, pp. 234-246. DOI: 10.1016/j.triboint.2016.04.019.

[11] Ghosh, S. and Rao, P.V. (2019). Comparison between sustainable cryogenic techniques and nano-MQL cooling mode in turning of nickel-based alloy. J. Cleaner Prod., 231, pp. 1036-1049. DOI: 10.1016/j.jclepro.2019.05.196.

[12] Makhesana, M.A., Patel, K.M. and Mawandiya, B.K. (2021). Environmentally conscious machining of Inconel 718 with solid lubricant assisted minimum quantity lubrication. Met. Powder Rep., 76, S24-S29. DOI: 10.1016/j.mprp.2020.08.008.

[13] Rajurkar, A. and Chinchanikar, S. (2022). Experimental Investigation on Laser-Processed Micro-Dimple and Micro-Channel Textured Tools during Turning of Inconel 718 Alloy. J. Mater. Eng. Perform., 31(5), pp. 4068-4083. DOI: 10.1007/s11665-021-06493-7.

[14] Rajurkar, A. and Chinchanikar, S. (2021). Performance study of dimple and channel textured tools during turning of Inconel-718. Mater. Today Proc., 46(17), pp. 8347-8351. DOI: 10.1016/j.matpr.2021.03.399.

[15] Ahmed, W., Hegab, H., Mohany, A. and Kishawy, H. (2021). On machining hardened steel AISI 4140 with self-propelled rotary tools: Experimental investigation and analysis. Int. J. Adv. Manuf. Technol., 113(11-12), pp. 3163-3176. DOI: 10.1007/s00170-021-06827-8.

[16] Wang, Z.M. Ezugwu, E.O. and Gupta, A. (1998). Evaluation of a self-propelled rotary tool in the machining of aerospace materials. Tribol. Trans., 41(2), pp. 289-295. DOI: 10.1080/10402009808983750.

[17] Kishawy, H.A., Becze, C.E. and McIntosh, D.G. (2004). Tool performance and attainable surface quality during the machining of aerospace alloys using self propelled rotary tools. J. Mater. Process. Technol., 152(3), pp. 266-271. DOI: 10.1016/j.jmatprotec.2003.11.011.

[18] Sasahara, H., Kato, A., Nakajima, H., Yamamoto, H., Muraki, T. and Tsutsumi, M. (2008). High-speed rotary cutting of difficult-to-cut materials on multitasking lathe. Int. J. Mach. Tools Manuf., 48(7-8), pp. 841-850. DOI: 10.1016/j.ijmachtools.2007.12.002.

[19] Dessoly, V., Melkote, S.N. and Lescalier, C. (2004). Modeling and verification of cutting tool temperatures in rotary tool turning of hardened steel. Int. J. Mach. Tools Manuf., 44(14), pp. 1463–1470. DOI: 10.1016/j.ijmachtools.2004.05.007.

[20] Uhlmann, E., Kaulfersch, F. and Roeder, M. (2014). Turning of high-performance materials with rotating indexable inserts. Procedia CIRP, 14, pp. 610-615. DOI: 10.1016/j.procir.2014.03.028.

[21] Ezugwu, E.O. (2007). Improvements in the machining of aero-engine alloys using self-propelled rotary tooling technique. J. Mater. Process. Technol., 185(1-3), pp. 60-71. DOI: 10.1016/j.jmatprotec.2006.03.112.

[22] Kossakowska, J. and Jemielniak, K. (2012). Application of Self-Propelled Rotary Tools for turning of difficult-to-machine materials. Procedia CIRP, 1, pp. 425–430. DOI: 10.1016/j.procir.2012.04.076.

[23] Chinchanikar, S. and Gadge, M. (2024). Modelling cutting force for turning AISI 304 stainless steel with PVD-AlTiN coated, PVD-AlTiN coated-microblasted, and MTCVD-TiCN/Al_2O_3 coated tools. Advances in Materials and Processing Technologies, pp. 1-26. DOI: 10.1080/2374068X.2024.2341512.

[24] Kulkarni, P. and Chinchanikar, S. (2024). Machining effects and multi-objective optimization in Inconel 718 turning with unitary and hybrid nanofluids under MQL. Frattura ed Integrità Strutturale, 68, pp. 222-241. DOI: 10.3221/IGF-ESIS.68.15.

[25] Chinchanikar, S. and Gadge, M. (2024). Investigations on tool wear behavior in turning AISI 304 stainless steel: An empirical and neural network modeling approach. Frattura ed Integrità Strutturale, 18(67), pp. 176-191. DOI: 10.3221/IGF-ESIS.67.13.